Proc. Natl. Acad. Sci. USA
Vol. 94, pp. 12676–12681, November 1997
Neurobiology

Ultrastructural localization of zinc transporter-3 (ZnT-3) to synaptic vesicle membranes within mossy fiber boutons in the hippocampus of mouse and monkey

H. JÜRGEN WENZEL*, TOBY B. COLE†, DONALD E. BORN‡, PHILIP A. SCHWARTZKROIN*§, AND RICHARD D. PALMITER†¶

Departments of *Neurological Surgery, ‡Pathology, §Physiology/Biophysics, and †Biochemistry and †Howard Hughes Medical Institute, Box 357370, University of Washington, Seattle, WA 98195

Contributed by Richard D. Palmiter, September 9, 1997

ABSTRACT **Zinc transporter-3 (ZnT-3), a member of a growing family of mammalian zinc transporters, is expressed in regions of the brain that are rich in histochemically reactive zinc (as revealed by the Timm's stain), including entorhinal cortex, amygdala, and hippocampus. ZnT-3 protein is most abundant in the zinc-enriched mossy fibers that project from the dentate granule cells to hilar and CA3 pyramidal neurons. We show here by electron microscopy that ZnT-3 decorates the membranes of all clear, small, round synaptic vesicles (SVs) in the mossy fiber boutons of both mouse and monkey. Furthermore, up to 60–80% of these SVs contain Timm's-stainable zinc. The coincidence of ZnT-3 on the membranes of SVs that accumulate zinc, and its homology with known zinc transporters, suggest that ZnT-3 is responsible for the transport of zinc into SVs, and hence for the ability of these neurons to release zinc upon excitation.**

Most of the zinc in the mammalian brain is associated with metalloproteins; however, there is also a pool of histochemically reactive zinc that exists in synaptic vesicles (SVs) of a subset of glutamatergic neurons, which has led to classification of these neurons as zinc-containing or zinc-ergic (1–4). Pathways utilizing this vesicular form of zinc have been mapped using histochemical stains such as the neo-Timm's sulfide-silver method (5), selenium stain (6, 7), and the fluorescent compound, TSQ (8). One of the best described zinc-ergic systems is found in the rodent hippocampal formation, where vesicular zinc can be detected in each component of the trisynaptic circuit that includes (*i*) perforant path projections from the entorhinal cortex to the outer molecular layer of the dentate gyrus, (*ii*) mossy fiber (MF) projections from granule cells in the dentate gyrus to hilar neurons and pyramidal cells in the CA3 region (4, 9–11), (*iii*) projections from CA3 pyramidal neurons to neurons in the CA1 region, and (*iv*) projections from CA1 to subiculum (3, 4). Electron microscopy (EM) has revealed that the Timm's stain precipitate is present within SVs in the giant axonal boutons of the MFs in the hilus and stratum (s.) lucidum (1, 2, 12). However, only ≈10–15% of the SVs within a given bouton have been shown to contain Timm's precipitate (2); thus, it has been difficult to ascertain whether zinc is present in a subset of vesicles or if it is present in the same vesicles as glutamate.

Accumulation of zinc within SVs presumably depends on the action of specific transporters, by analogy with the accumulation of other neurotransmitters in SVs (13). A gene, designated zinc transporter-3 (*ZnT3*), homologous to two established zinc transporters (14, 15) was recently cloned (16). ZnT-3 was shown by *in situ* hybridization to be expressed at high levels in hippocampus and neocortex. Immunocytochemical studies demonstrated its localization to the MFs, where the histochemical Timm's reaction has revealed zinc-containing SVs. This profile suggested that ZnT-3 might be the vesicular zinc transporter responsible for sequestration of zinc in MF SVs (16), but also raised questions regarding the ultrastructural localization of ZnT-3 relative to zinc and other neurotransmitters.

MATERIALS AND METHODS

Tissue Preparation. Eight mice (6 C57BL/6; 2 C57BL/6x129), ages 8–20 weeks, and five monkeys, (*Macaca nemestrina*), age 1 year were used for light microscopy and EM immunocytochemical localization of ZnT-3 and for histochemical localization of zinc within the MF system of the hippocampus.

Mice were anesthetized with Nembutal (100 mg/kg, i.p.), then perfused with isotonic saline with heparin (100 units/ml saline), followed by 4% paraformaldehyde in 0.1 M sodium phosphate buffer (PB), pH 7.4, or by a solution containing 4% paraformaldehyde, 0.1% glutaraldehyde, and 0.1% picric acid in PB. [The low level of glutaraldehyde was necessary to preserve immunoreactivity (IR) but resulted in suboptimal ultrastructure.] The brains were removed and placed in the same fixative for 4 hr at 4°C. Monkeys were anesthetized (Nembutal, 50–75 mg/kg) and perfused transcardially with 4% paraformaldehyde in PB. Tissue blocks from the temporal lobe, containing the hippocampus, were dissected and cut into 1.5-mm thick slices that were then placed in the same fixative for 24 hr at 4°C.

After postfixation, the brains (mice) or slices (monkey) were rinsed in PB, cryoprotected in 10% sucrose for 1 hr, followed by 30% sucrose for 8–12 hr at 4°C, then frozen on dry ice. Transverse serial sections, 30 μm for light microscopy and 80 μm for EM, were cut on a sliding microtome equipped with a freezing stage, and sections were selected for further processing.

EM Detection of ZnT-3. An affinity-purified rabbit antibody specific for ZnT-3 (16) was used to determine its ultrastructural localization. Sections were rinsed in PB, followed by 0.1 M Tris·HCl buffer (TB), pH 7.4; then endogenous peroxidases were inactivated by treatment with 0.5–1% H_2O_2 in TB for 2 hr. Sections were treated with 3% BSA, 3% goat serum, and 0.25% dimethyl sulfoxide in TBS (0.05 M TB/0.15 M NaCl, pH 7.4) for 1 hr to reduce nonspecific staining. Sections were rinsed in TBS for 30 min and incubated for 20 hr at 4°C in ZnT-3 antiserum, diluted 1:100 to 1:300 in TBS containing 1% goat serum, 2% BSA and 0.25% dimethyl sulfoxide. Following rinses for 2 hr in TBS, sections were incubated in biotinylated goat anti-rabbit IgG (diluted 1:500) for 24 hr at 4°C, rinsed 2 hr in TBS and then incubated in ABC (Elite ABC Kit; Vector

The publication costs of this article were defrayed in part by page charge payment. This article must therefore be hereby marked "*advertisement*" in accordance with 18 U.S.C. §1734 solely to indicate this fact.

Abbreviations: SV, synaptic vesicle; MF, mossy fiber; MFB, MF bouton; IR, immunoreactivity; ZnT-3, zinc transporter-3; EM, electron microscopy; s., stratum; GABA, γ-aminobutyric acid.

¶To whom reprint requests should be addressed. e-mail: palmiter@u.washington.edu.

Laboratories), diluted 1:500 in 1% goat serum, 2% BSA, 0.25% dimethyl sulfoxide and TBS for 24 hr at 4°C. Sections were rinsed in TB (pH 7.6), then incubated for 15 min in 0.025% 3,3′-diaminobenzidine in TB. After reaction for 5–10 min in fresh 3,3′-diaminobenzidine with 0.003% H_2O_2, sections were rinsed in TB, followed by PB. Specificity of the immunostaining was evaluated by omitting primary antibody.

Sections were further processed for EM by postfixation in 1% osmium tetroxide in PB for 1 hr at 22°C, followed by alcohol dehydration and flat embedding in Eponate 12 (Ted Pella, Redding, CA) between two aclar sheets for 24 hr at 60°C. Selected immunoreactive areas were cut from embedded sections and remounted with Eponate 12 on plastic blocks. Serial ultrathin sections were cut close to the tissue surface, stained with uranyl acetate and lead citrate, and examined on a Philips (Eindhoven, The Netherlands) 410 electron microscope.

Postembedding Detection of ZnT-3 and Glutamate. To investigate colocalization of ZnT-3 and glutamate in SVs of MFs, postembedding immunocytochemistry was performed as described by Wenzel *et al.* (17). Ultrathin sections from Timm's-stained sections or glutaraldehyde/paraformaldehyde-fixed tissue were etched with redox reagents (periodic acid, sodium metaperiodate) to reduce osmium staining and to expose antigenic sites. Sections were then incubated with the primary antibodies—rabbit anti-glutamate (Sigma) diluted 1:10,000 or affinity-purified ZnT-3 antibody, diluted 1:50 or 1:100—followed by goat-anti-rabbit IgG conjugated to gold (10 nm, Ted Pella), diluted 1:20.

Timm's Staining. For light microscopy detection in mouse and monkey brains, a Timm's-staining protocol described by Franck *et al.* (18) was adapted. Fixed hippocampal slices (1 mm) were immersed in 0.4% Na_2S for 30 min, then fixed ~16 hr in 1% paraformaldehyde and 1.25% glutaraldehyde. The fixed slices were cryoprotected, 30 μm sections were mounted and dried, and sections were immersed in developer [30 ml gum Arabic (50%), 5 ml citrate buffer (2 M, pH 3.7), 15 ml hydroquinone (5.67%) and 0.25 ml $AgNO_3$ (17%)] for at least 60 min. A brief staining period was used in most cases to focus on the densely reactive MF pathway; longer exposure times revealed typical laminar Timm's profile in the dentate molecular layer (not shown).

To increase the specific staining of zinc and improve visualization of the MF system by EM, a variant of the neo-Timm's stain (2, 5, 19, 20) was modified. After the initial fixation, the tissue was transferred to a solution containing 3–4% glutaraldehyde, 0.1% Na_2S, and 0.136 mM $CaCl_2$ in 0.12 M Millonig's buffer, pH 7.3, for 24 hr at 4°C. The tissue was transferred to cold 0.12 M Millonig's buffer with 0.136 mM $CaCl_2$ and sectioned with a vibratome at 80 μm. Sections containing the hippocampus were transferred to a fresh developing solution [60 ml gum Arabic (50%), 10 ml 2 M citrate buffer; 15 ml hydroquinone (5.67%) and 15 ml silver lactate (0.73%)] for 1 hr in the dark, with constant agitation (20), then washed for 10 min and postfixed in phosphate-buffered osmium tetroxide for 1 hr. The tissue was dehydrated through alcohols to propylene oxide, then flat-embedded in Eponate 12.

RESULTS

Morphological Characteristics of MF Boutons (MFBs) in Mouse and Monkey. MF axons of the dentate granule cells establish synaptic contacts with neurons in the dentate hilus and with pyramidal cells of the hippocampal CA3 region (see refs. 21 and 22 for reviews). MF axons ramify within the hilus, and form unmyelinated axon bundles in the CA3 region, forming a major band above the pyramidal cell bodies (s. lucidum) and ramifying within and below the pyramidal cell layer (s. pyramidale and s. oriens, respectively) see Figs. 1*A*; 2*A* and refs. 22 and 23. MF distribution is similar in monkey and rat hippocampus, although there are differences in MF trajectories between primates and rodents (24). The characteristic ultrastructural appearance of MF synaptic boutons is seen in both rat and monkey (24). In our study, features of MFs and their terminals in the mouse and monkey hippocampus were consistent with previous descriptions (see Figs. 1 and 2). The MFs form two types of boutons; some are relatively small terminals, whereas others are larger and more irregular in shape, with smaller vesicle-filled extensions arising from a large varicosity. Both types of boutons have regions filled with densely packed, clear, spherical SVs (35–45 nm in diameter); a few dense core vesicles (60–140 nm); mitochondria; tubules of the smooth endoplasmic reticulum; and occasional microtubules, neurofilaments, and large clear vesicles (60–200 nm) (23, 25). In both the mouse and the monkey, the large MFBs make two types of specialized contacts with CA3 pyramidal cells and hilar neurons: (*i*) symmetrical desmosome-like, nonsynaptic junctions (puncta adherentia), characterized by symmetrical densities in association with the proximal dendritic shafts of CA3 pyramidal cells in s. lucidum (Figs. 2*D*, 3 *B* and *C*); and (*ii*) asymmetrical synapses with complex branching and invaginating spines, called "thorny excrescences" by Cajal (26), arising from dendritic shafts and somata of CA3 and hilar neurons (Figs. 1 *E* and *F*; 2 *E* and *F*, and 3*A*). For comparison with the rat hippocampus, see ref. 25.

Localization of ZnT-3 and Zinc in MFBs from Mice. In sections of mouse hippocampus stained with antiserum to ZnT-3, intense IR was observed within the MF system (Fig. 1*B*). In particular, those regions where MFBs contact the somata and dendrites of hilar neurons and CA3 pyramidal cells stained intensely with the ZnT-3 antiserum. This pattern of ZnT-3 IR was identical to the histochemical localization of zinc by the Timm's reaction (Fig. 1*A*) and included suprapyramidal MFBs forming an immunoreactive band in the s. lucidum (arrow in Fig. 1*B*) reaching from the hilus to CA3a, and intrapyramidal and infrapyramidal MFBs, the latter primarily within the CA3c subregion (Fig. 1*B*). S. radiatum and s. oriens of CA1 also stained for ZnT-3, as did the dentate outer molecular layer; the dentate inner molecular layer showed only light staining with the antibody (Fig. 1*B*). Control sections not exposed to the primary ZnT-3 antibody showed no IR (Fig. 3*C*).

At the EM level, ZnT-3 IR was observed in MFBs within the hilus and the CA3 subregion (Figs. 1 *D* and *F*). The intense ZnT-3 IR corresponded exclusively to MFBs; SVs of interneurons in the same sections were not stained (Fig. 1*D*). Electron micrographs of MFBs at higher magnification (Fig. 1*F*) revealed that ZnT-3 IR was localized uniformly to the membranes of spherical, clear (agranular) SVs. ZnT-3 IR associated with round clear SVs was similar in both the small boutons on dendritic shafts (Fig. 3*B*), and large boutons associated with complex spines (Figs. 1*F* and 3*A*). MFBs sampled from different locations in the hilus and the CA3 subregion showed no difference in the pattern or intensity of ZnT-3 IR. In the outer molecular layer of the dentate gyrus, less intense ZnT-3 IR was observed on SVs in some axon terminals (Fig. 3*D*).

EM of Timm's-stained hippocampal sections revealed Timm's silver precipitate in regions corresponding to the MFBs (Fig. 1*C*). At higher magnification, it was apparent that up to 60–80% of the SVs of MFBs contain silver granules (Fig. 1*E*). In experiments in which immunocytochemical staining for ZnT-3 was carried out in Timm's-stained ultrathin sections (using postembedding techniques), the ZnT-3 associated gold particles were found exclusively over Timm's-positive MFBs (Fig. 3*G*). In addition, ultrathin sections reacted with an antibody against glutamate revealed glutamate IR in MFBs (Fig. 3*H*).

Localization of ZnT-3 and Zinc in Monkey Hippocampus. Using ZnT-3 immunocytochemistry, the pattern of MF collateral extension outside the hilar region was somewhat different in primates compared with mice (compare Figs. 1*B* and 2*B*). In the monkey, MFBs that stain with Timm's reaction product (Fig. 2*A*) and ZnT-3 antibody (Fig. 2*B*) occupy the hilus and entire CA3 region. Outside the MF system, ZnT-3 IR

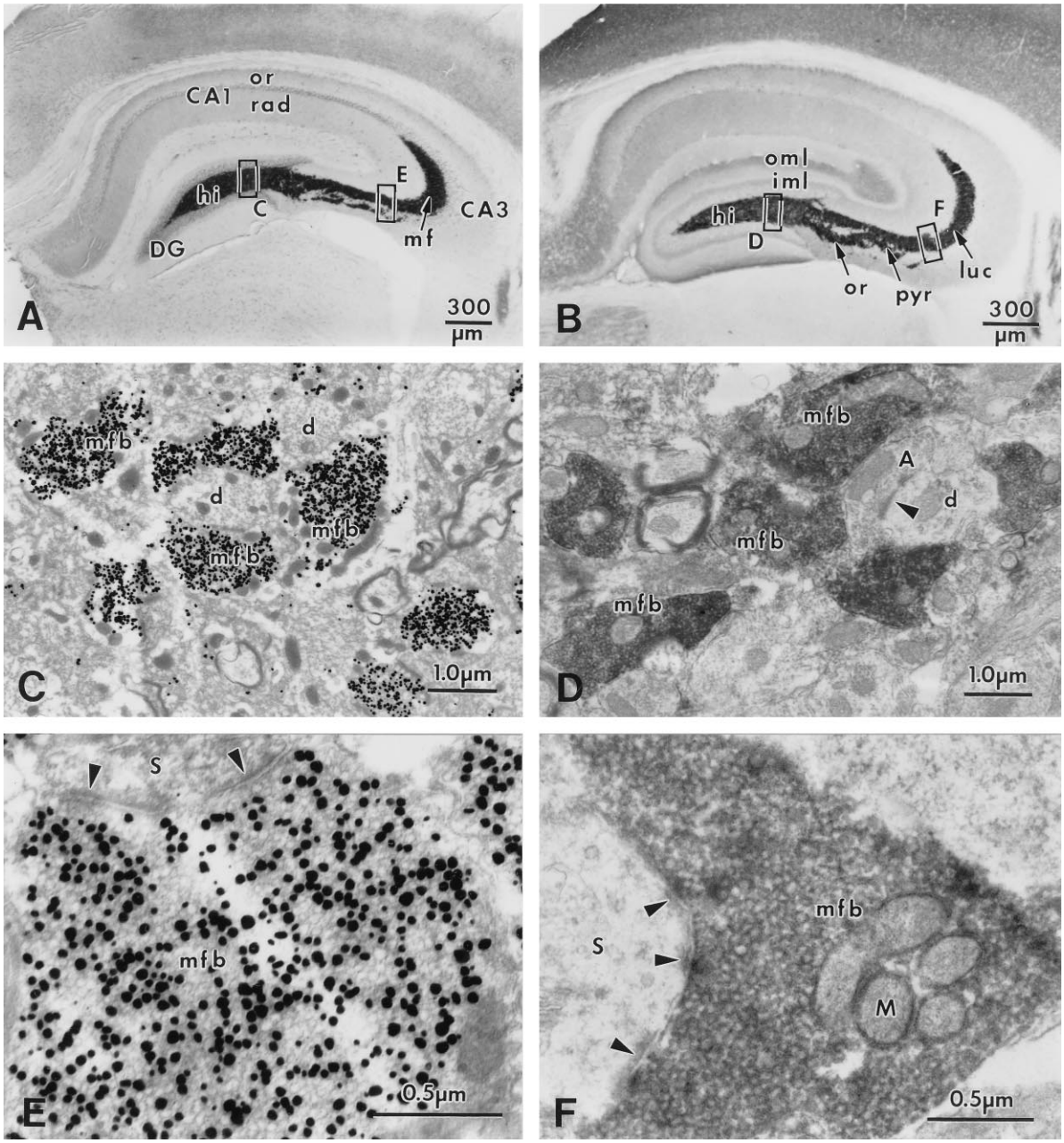

FIG. 1. Localization of histochemically reactive zinc (*A, C, E*) and IR for ZnT-3 protein (*B, D, F*) in the mouse hippocampus. (*A*) Transverse section of the hippocampus demonstrating intense reaction product in the mossy fiber (MF) system (dark band labeled "mf") after Timm's staining procedure; counterstained with cresyl violet. Note the lighter laminar staining in s. radiatum (rad) and oriens (or) of CA1. (*B*) Transverse section of the hippocampus reacted with an affinity-purified antiserum against ZnT-3 protein. IR is intense in the zinc-containing MF projections; arrows indicate ZnT-3 staining in s. lucidum (luc), pyramidale (pyr) and oriens (or) of CA3. The dentate outer (oml) and inner (iml) molecular layers, and s. radiatum (rad) and oriens (or) of CA1 also appear lightly immunoreactive for ZnT-3. (*C*) Electron micrograph from the dentate hilus (indicated area in *A*) showing MF boutons (mfb) with high density of silver granules. (*D*) Electron micrograph from the dentate hilus (indicated area in *B*) showing intense ZnT-3 IR in MFBs (mfb). Note the probable interneuron terminal (*A*) without ZnT-3 IR, making a symmetric synaptic contact (arrowhead) onto a dendrite (d). (*E, F*) Higher magnification of MFBs from CA3 s. lucidum (indicated areas in *A* and *B*) to demonstrate the vesicular localization of zinc (*E*) and ZnT-3 IR on synaptic vesicle membranes (*F*). Other abbreviations: CA1, CA3 hippocampal regions; DG, dentate gyrus; hi, hilus; M, mitochondrion; S, spine; arrowhead, synaptic contact.

was observed in a prominent band in the dentate inner molecular layer (but not the outer molecular layer); staining was also observed in s. radiatum and s. oriens of the CA1 region (Fig. 2*B*). At the EM level, the synaptic and nonsynaptic junctions between MFBs and dendritic shafts, somata, and thorny excrescences of CA3 pyramidal cells were similar to those seen in mice (Figs. 2 *D* and *F*; 3 *A* and *B*). Although MFBs were larger in size and exhibited more synaptic contacts per bouton in monkey than in mouse, there was no obvious difference in SV populations or in the localization of ZnT-3 IR to the vesicle membrane; the clear spherical SVs revealed ZnT-3 IR associated with vesicle membranes, irrespective of bouton size, location, or species (Figs. 1*F* and 2*F*). As in the mouse, EM of Timm's-stained sections of monkey hippocampus revealed silver precipitate in many SVs of MFBs, albeit less frequently than in mouse (Figs. 2 *C* and *E*).

DISCUSSION

This study reveals that ZnT-3 IR is localized to the membranes of all small, round, clear SVs of MFBs that have been shown

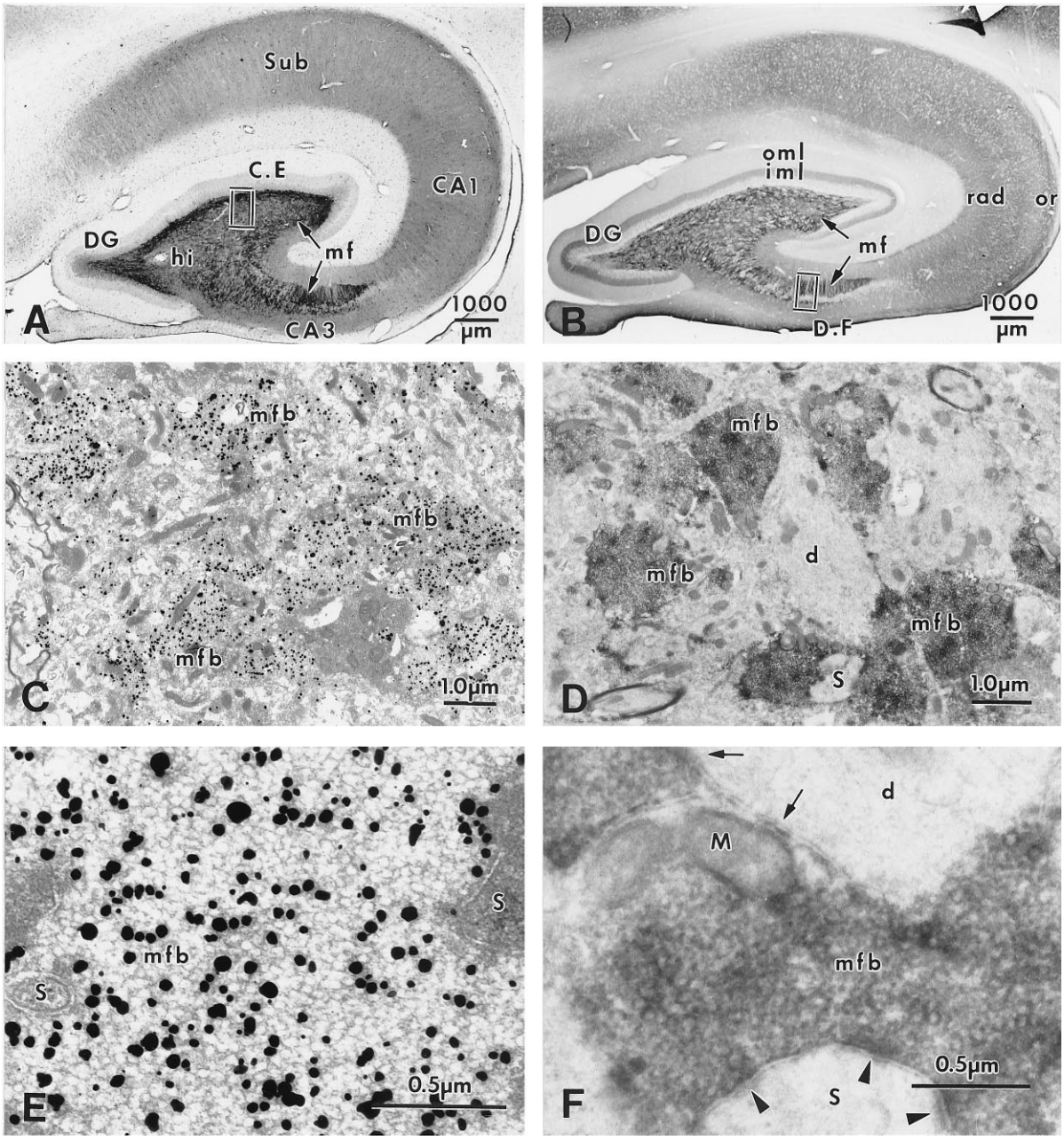

FIG. 2. Localization of histochemically reactive zinc (*A, C, E*) and IR for ZnT-3 protein (*B, D, F*) in the monkey hippocampus. (*A*) Frontal section of the hippocampus demonstrating intense Timm's stain for vesicular zinc in the MF projections (mf) within hilus and CA3. Lighter staining is seen in s. radiatum and oriens and subiculum (Sub). (*B*) Frontal section of the monkey hippocampus. ZnT-3 IR is present in the zinc-rich MF projections (mf) in hilus and CA3 region; lighter IR is seen in the dentate iml, in CA1 s. radiatum (rad) and oriens (or) and in subiculum. (*C*) Electron micrograph from the dentate hilus (indicated area in *A*) showing MFBs labeled with silver granules. (*D*) Electron micrograph from the s. lucidum (indicated area in *B*) demonstrating ZnT-3 IR in MFBs that surround a dendrite (d). (*E*) Higher magnification of part of a giant MFB in synaptic contact with spines in CA3 s. lucidum, showing dark silver granules located in the clear round SVs. (*F*) Higher magnification of a MFB in synaptic contact with a giant spine (arrowheads), also making nonsynaptic contacts onto a dendritic shaft (d, arrows). ZnT-3 IR is localized to the membranes of clear, round SVs within the bouton. Abbreviations as in Fig. 1.

previously to contain excitatory amino acids (17, 27). The majority (up to 60–80% in mouse MFBs) of these SVs also contain Timm's reaction product, indicative of vesicular zinc. The comparison of mouse to monkey revealed no species-related differences in the localization of ZnT-3 to SVs of MFBs, although there were differences in the general pattern of MF distribution. Synapses of nonglutamatergic local circuit neurons, e.g., hilar interneurons (Figs. 1*D*, 3 *E* and *F*), did not show ZnT-3 IR.

Recent studies demonstrate significant differences between rodents and primates with respect to dendritic length (28), the presence of basal dendrites (29), and basic ultrastructure (30). Our studies reveal another species difference in the pattern of MF projections to the pyramidal cells of the CA3 region. In mice, ZnT-3 and Timm's-positive MFBs were found in the hilus, s. lucidum, s. pyramidale between the CA3 pyramidal cells, and in s. oriens where MFBs were restricted to the CA3c subfield; in contrast, in the monkey hippocampus the MFBs that stain with Timm's reaction product and ZnT-3 antibody occupied the hilus and entire CA3 region. The appearance of large MFBs in s. lucidum and oriens in the monkey hippocampus is consistent with observations by Seress (24), who pointed out that large MFBs form synapses with both apical and basal parts of the dendritic tree in primates, whereas in rodents

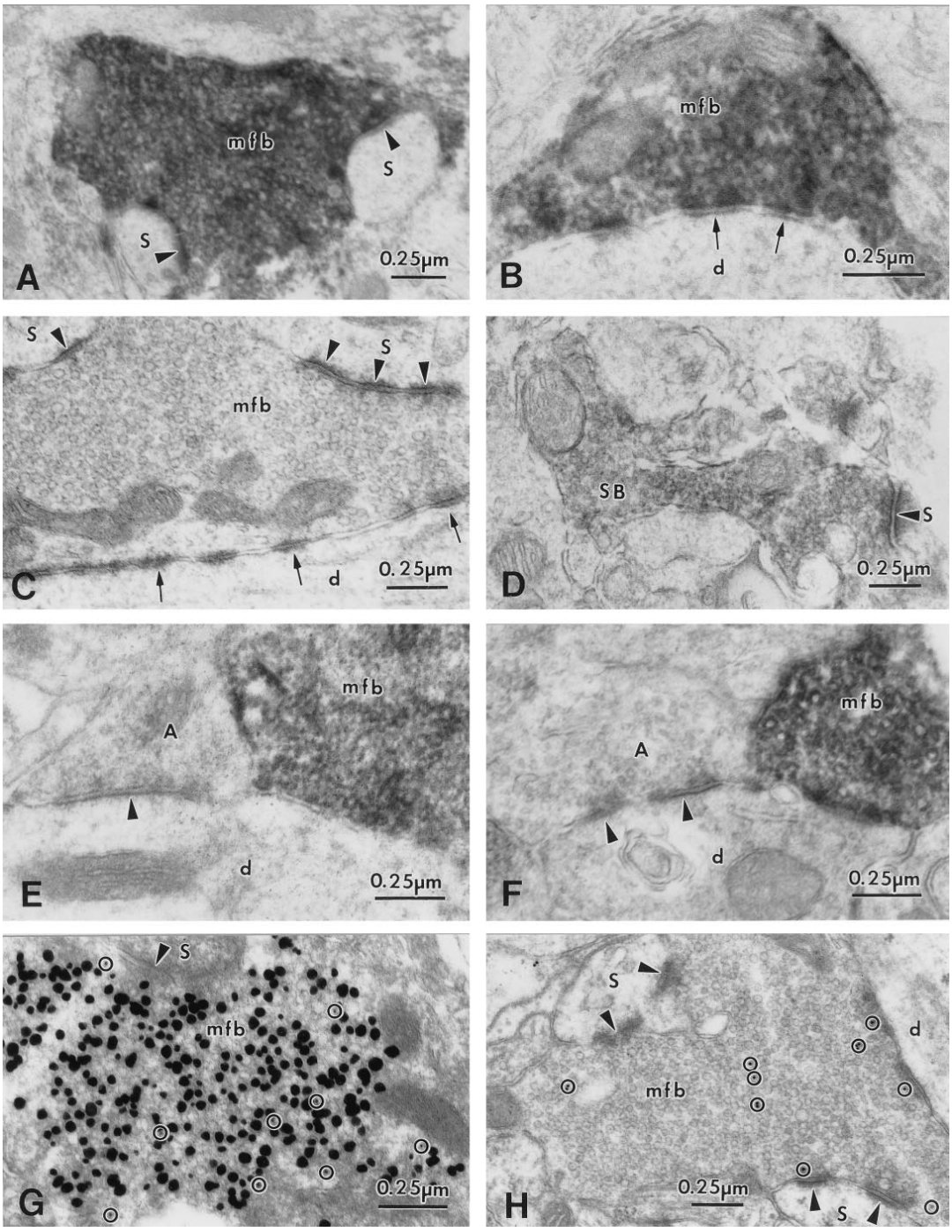

FIG. 3. Electron micrographs from the mouse and monkey (*E*) hippocampus showing ZnT-3 IR in terminals of glutamatergic projections. (*A*) ZnT-3 localization on clear, round SVs in a MFB in synaptic contact with spines (arrowheads). (*B*) ZnT-3 positive MFB making nonsynaptic contacts (arrows) onto a dendrite (d) in CA3 s. lucidum. (*C*) Control section of the CA3 s. lucidum in which the antibody against ZnT-3 protein was omitted; SVs in MFB (mfb) are devoid of ZnT-3 IR. The MFB forms synaptic contacts (arrowheads) with spines (s) and nonsynaptic contacts with a dendrite (d; arrows). (*D*) Synaptic bouton (SB) in the outer molecular layer of the dentate gyrus showing ZnT-3 IR on SV membranes. (*E*) and (*F*) Hilar dendrites (d) from the monkey (*E*) and mouse (*F*) hippocampus, contacted by MFBs with intense ZnT-3 IR. Adjacent presumably GABA-ergic terminals make symmetric synaptic contacts (arrowheads) and lack ZnT-3 IR on their SVs. (*G*) Part of a large MFB showing vesicular zinc (large silver granules) and ImmunoGold (Janssen) particles (10 nm, ○) corresponding to ZnT-3 protein labeled by a postembedding ImmunoGold procedure. (*H*) MFB with ImmunoGold-labeling for glutamate (10 nm particles, ○) demonstrating glutamate as the neurotransmitter of MF projections. Abbreviations as in Fig. 1.

synapses with large complex spines are seen only in s. lucidum. Another difference in the pattern of ZnT-3 IR (and Timm's) was observed in the dentate molecular layer. In mice, synapses of the perforant path showed ZnT-3 IR in the outer molecular layer, whereas in the monkey the inner molecular layer stained more intensely with the ZnT-3 antibody.

Evidence obtained from kinetic studies of zinc turnover and histochemical studies of zinc-containing boutons suggest that zinc is sequestered in SVs, and is released from boutons during normal activity by exocytosis of the zinc-filled vesicles (3). A zinc transporter localized to the SV membrane would provide an effective means of loading the SVs, and would be consistent with both light microscopy studies showing ZnT-3 staining pattern overlapping the MF distribution (16) and with the ultrastructural data showing its presence on SV membranes. Various brain regions containing zinc-ergic neurons have been

examined using EM techniques after neo-Timm's or selenium staining, and in all cases the reaction product is restricted to the presynaptic boutons of neurons (3, 19, 31). In addition, Timm's-stainable zinc is also present in nonneuronal cells in the brain, e.g., in the choroid plexus. Earlier ultrastructural investigations demonstrated that the zinc in synaptic boutons is localized in the vicinity of presynaptic vesicles (1, 12) and more recent studies indicate that the zinc is within individual vesicles (2, 19). However, previous work indicated that only a small fraction of clear, round vesicles in MFBs were reactive for zinc (1–3), suggesting that a subclass of vesicles might contain zinc. In contrast, our study of Timm's-stained material demonstrates that the majority of SVs in MFBs contain zinc, consistent with the observation that all SVs were ZnT-3 positive, and thus presumably capable of facilitating zinc uptake. It seems likely that the lack of Timm's reaction product in individual SVs may represent vagaries of the methodology (e.g., rapidity of fixation), rather than absence of zinc. We suggest that all the SVs within MFBs contain both zinc and glutamate. In non-MFBs, e.g., boutons of entorhinal projections in the outer molecular layer of mouse (Fig. 3*D*), where both Timm's stainable zinc and ZnT-3 IR are less intense, all SVs still appear to react with the antibody. We suggest that the level of ZnT-3 expression may vary in different zinc-ergic neurons, but that all of their clear SVs are able to accumulate zinc, perhaps proportionally to the density of ZnT-3; thus, the amount of zinc in SVs would reflect ZnT-3 density. Clearly, zinc is not an obligatory component of SVs containing excitatory amino acids, because Timm's staining is not observed in many glutamatergic neurons (for review see Frederickson, ref. 3). It is not clear what signals direct ZnT-3 to SVs of MFBs. It is also not known whether ZnT-3 can associate with different types of SVs (e.g. clear vs dense core vesicles). Thus, it is possible that ZnT-3 expression in neurons that produce different kinds of vesicles could result in sequestration of zinc in one population of SVs but not another. When ZnT-3 that was tagged with green fluorescent protein was expressed in baby hamster kidney cells it was clearly associated with vesicles; however, ZnT-3 did not facilitate zinc sequestration in baby hamster kidney cells, unlike ZnT-2 expressed in these same cells (15, 16); thus, other components of SVs may be necessary for zinc transport by ZnT-3.

Zinc is capable of modulating a variety of voltage and ligand-gated ion channels at physiological concentrations (5–500 μM; ref. 32). Zinc inhibition of *N*-methyl-D-aspartate-type glutamate receptors has been reported by many authors (33–35), and variable effects of zinc have been observed on non-*N*-methyl-D-aspartate glutamate receptors (33, 34, 36, 37). Zinc has also been shown to exert a powerful modulatory inhibition of γ-aminobutyric acid $(GABA)_A$ receptors (38). The MF system is particularly interesting considering the role that zinc might play in modulating transmitter-mediated actions. First, the MFBs have presynaptic kainate receptors (39), and zinc modulation of kainate-induced currents appears to be sensitive to synaptic calcium levels, which may vary in an activity-dependent manner (40). Second, α-amino-3-hydroxy-5-methyl-4-isoxazolepropionic acid receptors are associated with synaptic contacts made by MF onto hilar mossy cells and CA3 pyramidal cells (41–43). Third, *N*-methyl-D-aspartate and GABA receptor-mediated inputs to CA3 pyramidal cells occur in s. radiatum and oriens, with strong $GABA_A$ inhibition associated with somatically localized receptors (42, 44, 45). Further, in various forms of hippocampal pathology (e.g., mesial temporal sclerosis associated with temporal lobe epilepsy), there is a sprouting of zinc-rich MFs back on to the granule cells of origin (18, 20, 46, 47). Their aberrant terminal localization and their proximity to GABA receptors have prompted investigators to postulate a role for zinc in the breakdown of inhibition that is associated with seizure generation in epileptic hippocampus (48). All of these receptors are probably within range of zinc diffusion, especially after high levels of activity that release large amounts of zinc. Given so many potential "targets," the role of zinc in modulating the receptor responses to transmitter release during normal synaptic transmission remains to be resolved. Inactivation of ZnT-3 by gene-targeting will help define the role of zinc in modulating synaptic activities in the central nervous system.

The authors thank Norma L. Anderson, Paul Schwartz, and Janet Schukar, for excellent technical assistance. We thank C. J. Frederickson for reviewing the manuscript. This work was supported in part by National Institutes of Health Grant NS18895 (P.A.S.) and U.S. Public Health Service National Research Service Award T32 GM07270 (T.B.C.).

1. Haug, F.-M. Š. (1967) *Histochemie* **8,** 355–368.
2. Pérez-Clausell, J. & Danscher, G. (1985) *Brain Res.* **337,** 91–98.
3. Frederickson, C. J. (1989) *Int. Rev. Neurobiol.* **31,** 145–238.
4. Slomianka, L. (1992) *Neuroscience* **48,** 325–352.
5. Danscher, G. (1981) *Histochemistry* **71,** 1–16.
6. Danscher, G. (1984) in *The Neurobiology of Zinc*, eds. Frederickson, C. J., Howell, G. A. & Kasarskis, E. J. (Riss, New York), Vol. B, pp. 171–191.
7. Slomianka, L., Danscher, G. & Frederickson, C. J. (1990) *Neuroscience* **38,** 843–854.
8. Frederickson, C. J., Kasarskis, E. J., Ringo, D. & Frederickson, R. E. (1987) *J. Neurosci. Methods* **20,** 91–103.
9. Haug, F.-M. Š., Blackstad, T. W., Simonsen, A. H. & Zimmer, J. (1971) *J. Comp. Neurol.* **142,** 23–32.
10. Crawford, I. L. & Connor, J. D. (1972) *J. Neurochem.* **19,** 1451–1458.
11. Zimmer, J. & Haug, F.-M. Š. (1978) *J. Comp. Neurol.* **179,** 581–618.
12. Ibata, Y. & Otsuka, N. (1969) *J. Histochem. Cytochem.* **17,** 171–175.
13. Borowsky, B. & Hoffmann, B. J. (1995) *Int. Rev. Neurobiol.* **38,** 139–199.
14. Palmiter, R. D. & Findley, S. D. (1995) *EMBO J.* **14,** 639–649.
15. Palmiter, R. D., Cole, T. B. & Findley, S. D. (1996) *EMBO J.* **15,** 1784–1791.
16. Palmiter, R. D., Cole, T. B., Quaife, C. J. & Findley, S. D. (1996) *Proc. Natl. Acad. Sci. USA* **93,** 14934–14939.
17. Wenzel, H. J., Buckmaster, P. S., Anderson, N. L., Wenzel, M. E. & Schwartzkroin, P. A. (1997) *Hippocampus* **7,** in press.
18. Franck, J. E., Pokorny, J., Kunkel, D. D. & Schwartzkroin, P. A. (1995) *Epilepsia* **36,** 543–558.
19. Danscher, G. (1996) *Histochem. J.* **28,** 361–373.
20. Babb, T. L., Kupfer, W. R., Pretorius, J. K., Crandall, P. H. & Levesque, M. F. (1991) *Neuroscience* **42,** 351–363.
21. Frotscher, M., Soriano, E. & Misgeld, U. (1993) *Synapse* **16,** 148–160.
22. Amaral, D. G. & Witter, M. P. (1995) in *The Rat Nervous System*, ed. Paxinos, G. (Academic, San Diego), pp. 443–493.
23. Claiborne, B. J., Amaral, D. G. & Cowan, W. M. (1986) *J. Comp. Neurol.* **246,** 435–458.
24. Seress, L. (1992) in *The Dentate Gyrus and its Role in Seizures*, eds. Ribak, C. E., Gall, C. M. & Mody, I. (Elsevier, Amsterdam), pp. 3–28.
25. Amaral, D. G. & Dent, J. A. (1981) *J. Comp. Neurol.* **195,** 51–86.
26. Ramon y Cajal, S. (1893) *Ann. Soc. Esp. Hist. Nat.* **22,** 53–114.
27. Beaulieu, C., Dyck, R. & Cynader, M. (1992) *NeuroReport* **3,** 861–864.
28. Claiborne, B. J., Amaral, D. G. & Cowan, W. M. (1990) *J. Comp. Neurol.* **302,** 206–220.
29. Seress, L. & Frotscher, M. (1990) *J. Comp. Neurol.* **293,** 253–267.
30. Seress, L. & Ribak, C. E. (1992) *Brain Res.* **569,** 353–357.
31. Danscher, G., Howell, G., Pérez-Clausell, J. & Hertel, N. (1985) *Histochemistry* **83,** 419–422.
32. Smart, T. G., Xie, X. & Krishek, B. J. (1994) *Prog. Neurobiol.* **42,** 393–441.
33. Peters, S., Koh, J. & Choi, D. W. (1987) *Science* **236,** 589–593.
34. Westbrook, G. L. & Mayer, M. L. (1987) *Nature (London)* **328,** 640–643.
35. Christine, C. W. & Choi, D. W. (1990) *J. Neurosci.* **10,** 108–116.
36. Mayer, M. L., Vyklicky, L., Jr. & Westbrook, G. L. (1989) *J. Physiol. (London)* **415,** 329–350.
37. Hori, N., Galeno, T. & Carpenter, D. O. (1987) *Cell. Mol. Neurobiol.* **7,** 73–90.
38. Legendre, P. & Westbrook, G. L. (1991) *Mol. Pharmacol.* **39,** 267– 274.
39. Baude, A., Nusser, Z., Molnár, E., McIlhinney, R. A. & Somogyi, P. (1995) *Neuroscience* **69,** 1031–1055.
40. Dreixler, J. C. & Leonard, J. P. (1997) *Brain Res.* **752,** 170–174.
41. Schröder, H. (1993) *Hippocampus* **3,** 139–148.
42. Petralia, R. S., Wang, Y.-X. & Wenthold, R. J. (1994) *J. Neurosci.* **14,** 6102–6120.
43. Catania M. V., Tölle, T. R. & Monyer, H. (1995) *J. Neurosci.* **15,** 7046–7061.
44. Siegel, S. J., Brose, N., Janssen, W. G., Gasic, G. P., Jahn, R., Heinemann, S. F. & Morrison, J. H. (1994) *Proc. Natl. Acad. Sci. USA* **91,** 564–568.
45. Johnson, R. R., Jiang, X. & Burkhalter, A. (1996) *J. Comp. Neurol.* **368,** 335–355.
46. Sutula, T., Cascino, G., Cavazos, J., Parada, I. & Ramirez, L. (1989) *Ann. Neurol.* **26,** 321–330.
47. Isokawa, M., Levesque, M. F., Babb, T. L. & Engel, J., Jr. (1993) *J. Neurosci.* **13,** 1511–1522.
48. Buhl, E. H., Otis, T. S. & Mody, I. (1996) *Science* **271,** 369–373.